Available online at www.sciencedirect.com
ScienceDirect
Ceramics International 36 (2010) 283–290
CERAMICS INTERNATIONAL
www.elsevier.com/locate/ceramint

Bioactivity of ferrimagnetic $MgO–CaO–SiO_2–P_2O_5–Fe_2O_3$ glass-ceramics

Rajendra Kumar Singh, A. Srinivasan *

Department of Physics, Indian Institute of Technology Guwahati, Guwahati 781039, India

Received 26 June 2009; received in revised form 30 June 2009; accepted 27 July 2009
Available online 25 August 2009

Abstract

Glass-ceramics with compositions $4.5MgO(45-x)CaO34SiO_2 16P_2O_5 0.5CaF_2 xFe_2O_3$ (where $x = 0$, 5, 10, 15 and 20 wt.%) were obtained by heat-treatment of melt quenched glasses at 1050 °C. Hydroxyapatite, magnetite and wollastonite were identified as major crystalline phases in all the glass-ceramic samples containing iron oxide. Akermanite was detected in glass-ceramic samples with high iron oxide content. Evolution of magnetic properties in the glass-ceramic samples as a function of iron oxide concentration is correlated with the amount of magnetite phase. Bioactivity of the glass-ceramic samples treated for various time periods in simulated body fluid (SBF) was evaluated by examining the apatite layer formation on their surface using X-ray diffraction, Fourier transform infrared reflection spectroscopy, scanning electron microscopy and energy dispersive spectroscopy techniques. Increase in bioactivity was observed as the iron oxide content was increased. The results help in understanding the evolution of the apatite surface layer with respect to immersion time in SBF and composition of the glass-ceramic samples.

Keywords: B. X-ray methods; C. Magnetic properties; D. Glass-ceramics; E. Biomedical applications

1. Introduction

Bioceramics such as sintered hydroxyapatite [$Ca_{10}(PO_4)_6(OH)_2$] [1,2] and apatite–wollastonite (A–W) glass-ceramics [3] with bone-bonding properties have been developed as alternate implant material to bioglass™. A–W glass-ceramics obtained from $MgO–CaO–SiO_2–P_2O_5–CaF_2$ glass has excellent mechanical properties apart from being bioactive [4,5]. Recently, development of bioglass-ceramics containing a magnetic phase has received attention for application as thermoseed in hyperthermia treatment of cancer [6–8]. The interest in these materials started when $SiO_2–CaO–P_2O_5$ glasses containing iron oxide were found to yield ferrimagnetic glass-ceramics upon heat-treatment at elevated temperatures [7]. The magnetic properties of this bioceramic arise from magnetite (Fe_3O_4) crystallized from hematite present in the glass during heat-treatment. When this bioceramic is placed in the region of the tumor and is subjected to an alternating magnetic field, heat is generated by magnetic hysteresis loss [8]. The tumor is effectively heated and selectively destroyed when local temperatures of 42–45 °C are attained by this process [9–11]. Magnetic glass-ceramics with zinc ferrite in a $CaO–SiO_2$ glass matrix [9], Fe_3O_4 in $Na_2O–CaO–SiO_2–P_2O_5$ glass matrix [10–13], Fe_3O_4 in a $CaO–SiO_2$ glass matrix [14] have also been developed for this purpose. The bonding of bioactive glass and glass-ceramics to bone tissue is associated with a series of chemical interactions at the interface with the surrounding fluids and tissue. It has been shown that most of the bioactive glasses [4,15,16] and glass-ceramics [7,17–19] form a layer of a carbonate containing hydroxyapatite on their surface in the body and bond to the living bone through this apatite layer. This hydroxycarbonate apatite layer is chemically and structurally equivalent to the mineral phase in bone and is responsible for interfacial bonding. It has been demonstrated [20–22] that the same kind of apatite layer can also be formed on the surfaces of bioactive glasses and glass-ceramics in an acellular simulated body fluid (SBF) [23].

In this paper, we report the preparation and the results of a systematic investigation of magnetic and surface properties of $4.5MgO(45-x)CaO34SiO_2 16P_2O_5 0.5CaF_2 xFe_2O_3$ (where $x = 0$, 5, 10, 15 and 20 wt.%) ferrimagnetic bioglass-ceramics. This system consisting of the A–W glass composition and hematite is promising due to the proven high mechanical strength of the base glass. This series of glass-ceramics also

* Corresponding author. Tel.: +91 361 2582712; fax: +91 361 2690762.
E-mail addresses: k.rajendra@iitg.ernet.in (R.K. Singh), asrini@iitg.ernet.in (A. Srinivasan).

0272-8842/$36.00
doi:10.1016/j.ceramint.2009.07.028

provides an opportunity to understand the influence of CaO and Fe_2O_3 content on the bioactivity and magnetic property of these materials, which may yield biomaterials suitable for applications like targeted drug delivery.

2. Experimental

Glass samples with composition $4.5MgO(45-x)$-$CaO34SiO_2 16P_2O_5 0.5CaF_2 xFe_2O_3$ (where $x = 0$, 5, 10, 15 and 20 wt.%) were first prepared by melt quenching from high purity SiO_2, MgO, CaF_2, Fe_2O_3, $CaCO_3$ and $NH_4(H_2PO_4)$. Appropriate amounts of the above compounds were thoroughly mixed and calcined at 900 °C for 24 h and melted at 1550 °C for 2 h. The homogenized melt was then quenched by pouring on a copper plate. As-quenched glasses were then heat-treated in air at 1050 °C for 3 h to form the glass-ceramics. An X-ray diffractometer (Seifert 3003 T/T) was used to identify the crystalline phases present in the glass-ceramic samples. Room temperature magnetization measurements were carried out using a vibrating sample magnetometer (VSM, Lakeshore 7410). The magnetic hysteresis loop of the glass-ceramics was obtained for ±20 kOe (kA/m) and ±500 Oe magnetic field sweeps. Cut and polished glass-ceramic plates of dimension 10 mm × 10 mm × 2 mm were rinsed with acetone in an ultrasonic bath. In vitro bioactivity test was carried out by soaking the dried glass-ceramic plates in SBF. SBF was prepared by dissolving appropriate amounts of reagent grade NaCl, $NaHCO_3$, KCl, $K_2HPO_4{\cdot}3H_2O$, $MgCl_2{\cdot}6H_2O$, $CaCl_2$ and Na_2SO_4 in ion exchanged water as per the recipe of Kokubo et al. [23]. The SBF was buffered at a pH of 7.4 with 50 mM $(CH_2OH)_3CNH_2$ and 45 mM HCl and maintained at 36.5 °C in order to simulate near physiological conditions [23]. The SBF used in these studies has been successfully employed for in vitro studies on several bioactive glasses and glass-ceramics [14,15,24–28]. Glass-ceramic samples immersed in SBF were taken out after 1, 3, 7, 10, 20 and 30 days, lightly washed with acetone and analyzed using an X-ray diffractometer (Seifert 3003 T/T) equipped with a grazing incidence device, a Fourier transform infra-red reflection spectrometer (PerkinElmer Spectrum BX), a scanning electron microscope (SEM, Leo 1430VP) and a SEM based energy dispersive X-ray spectrometer.

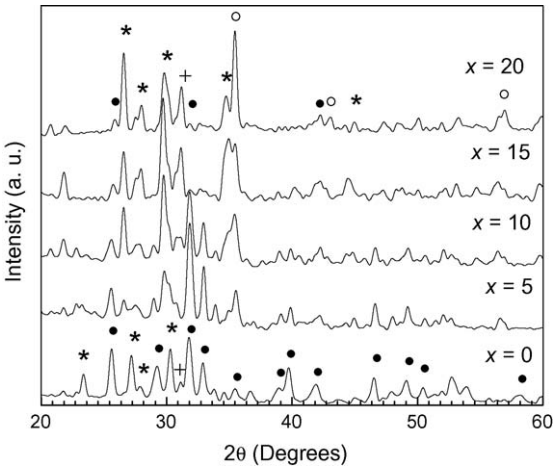

Fig. 1. XRD patterns of freshly prepared glass-ceramic samples. Crystalline phases present are magnetite (○), hydroxyapatite (●), wollastonite (*) and akermanite (+).

3. Results and discussion

X-ray diffraction (XRD) patterns of the glass-ceramic samples with different iron oxide content are shown in Fig. 1. Three major crystalline phases, *viz.*, hydroxyapatite [$Ca_{10}(PO_4)_6(OH)_2$, JCPDS file no. 74-0566], magnetite [Fe_3O_4, JCPDS file no. 88-0315] and wollastonite [$CaSiO_3$, JCPDS file no. 84-0655] were identified in all samples. An additional phase which was identified as akermanite [$Ca_2MgSi_2O_7$, JCPDS file no. 35-0592] developed in glass-ceramics with higher Fe_2O_3 content. Hydroxyapatite and wollastonite are bone minerals and their presence indicates the biocompatible nature of the glass-ceramics. Since the magnetite phase is expected to contribute to the magnetic properties of the glass-ceramics its average crystallite size was calculated from the broadening of the primary [(3 1 1)] peak in their XRD patterns using Scherrer's formula [29]. The average crystallite size of magnetite d, shows an increase from 20 (±0.41) to 31 (±0.61) nm as the iron oxide content is increased from 5 to 20 wt.% (Table 1). These glass-ceramic samples exhibit about 10% higher Vickers hardness number (VHN) as compared to CaO based glass-ceramics samples with the same iron oxide concentrations [30,31]. Presence of akermanite ($Ca_2MgSi_2O_7$) in these glass-ceramics increases the hardness of these glass-ceramics.

Table 1
Magnetic and structural parameters of glass-ceramics with composition $4.5MgO(45-x)CaO34SiO_2 16P_2O_5 0.5CaF_2 xFe_2O_3$.

Magnetic and structural parameters	Sample, x (wt.% of iron oxide)			
	5	10	15	20
Average (magnetite) crystallite size, d (nm)	20	22	26	31
Amount of magnetic phase (wt.%)	0.23	1.12	4.07	9.66
Saturation magnetization, M_s (emu/g)	0.21	1.03	3.75	8.89
Coercive field, H_C (Oe)	575	527	357	149
Remanent magnetization, M_r (emu/g)	0.03	0.08	0.77	0.81
Interpolated hysteresis area ± 20 kOe (erg/g)	348	1308	5171	6618
Interpolated hysteresis area ± 500 Oe (erg/g)	9	42	286	784

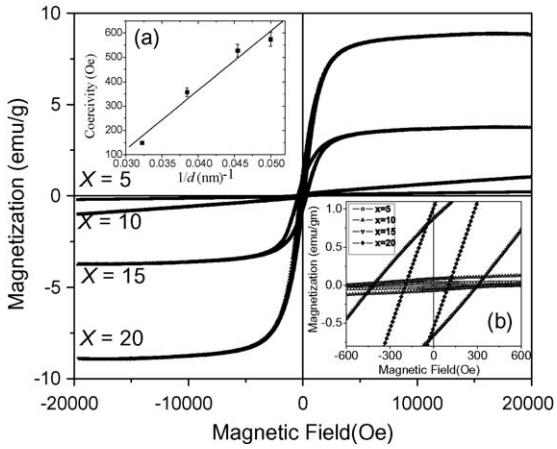

Fig. 2. Room temperature M–H curves of the glass-ceramics with different iron oxide content. Insets show (a) H_C versus $1/d$ plot, and (b) enlarged view of M–H loops near the origin.

Fig. 2 depicts the room temperature magnetic hysteresis (M–H) loops of the glass-ceramics with different iron oxide content. The coercive field (H_C) and the remanent magnetization (M_r) are individuated in the inset in Fig. 2. The magnetic field necessary to saturate the samples increases with increasing iron oxide content. The coercive field varies from 575 to 149 Oe, while the saturation magnetization varies from 0.21 to 8.89 emu/g over the composition range explored. The saturation magnetization (M_s) increases with the amount of magnetic phase in the sample. The highest amount of magnetite phase is obtained in the sample with $x = 20$, which also has the highest M_s. Amount of magnetic phase presented in the glass-ceramic samples was determined from the saturation magnetization ratio between the sample and pure magnetite ($M_s = 92$ emu/g [32]).

Fig. 3 summarizes the magnetic parameters obtained from the M–H loops of samples with different iron oxide content. M_s increases with increasing iron oxide concentration and shows a tendency to saturate for the sample with $x = 20$ (Fig. 3(a)). The increase of M_s with an increase in iron oxide concentration could be attributed to the increase in the amount of magnetite phase in the samples as observed in Fig. 1 and Table 1. On the other hand, H_C of the samples (Fig. 3(b)) decreases with increasing iron oxide concentration. H_C is influenced in a significant way by the crystal dimensions. The linear variation of H_C versus $1/d$ plot shown as an inset in Fig. 2 confirms the influence of crystalline size on the coercive field. Remanence signifies the nature of the magnetic material to be spontaneously magnetized, even in the absence of external magnetic field. Thus, the increase in M_r, M_s and hysteresis area, and the decrease in H_C with an increase in iron oxide content can be attributed to the increase in the amount and size of magnetite crystallites in the glass-ceramic samples. The area under the hysteresis loop increases with an increase in iron oxide content (Fig. 3(d)). Area under the loop is proportional to the energy loss and hence the heat generated by a sample subjected to an alternating field. The results obtained indicate that samples with higher iron oxide concentration are capable of generating more heat for the same magnetic field sweep. The large variation in the area under the loop for samples with $x = 5$ and 20 wt.% shows that controlled heat generation can be achieved at a constant field strength by appropriate choice of glass-ceramic composition. High magnetic fields of the order of ±20 kOe are difficult to realize in a clinical laboratory due to technical reasons. Therefore, room temperature hysteresis cycles were performed at much lower field amplitudes (i.e., ± 500 Oe) in order to evaluate the materials for hyperthermia applications. The corresponding M–H loops are shown in Fig. 4. It can be seen that the loop area drastically reduces when the magnetic field is reduced. However, all loop parameters scale down proportionally to the applied field amplitude. This shows that the properties of these glass-ceramics are preserved even at clinically amenable low magnetic fields.

In vitro dissolution of the glass-ceramics samples in SBF was undertaken in order to observe the material behavior in the vitro environment and to understand the basic mechanisms operating in the dissolution of the sample in SBF. Fig. 5(a) shows the grazing incidence XRD (GI-XRD) patterns from the surface of the glass-ceramics sample with $x = 15$ wt.% iron

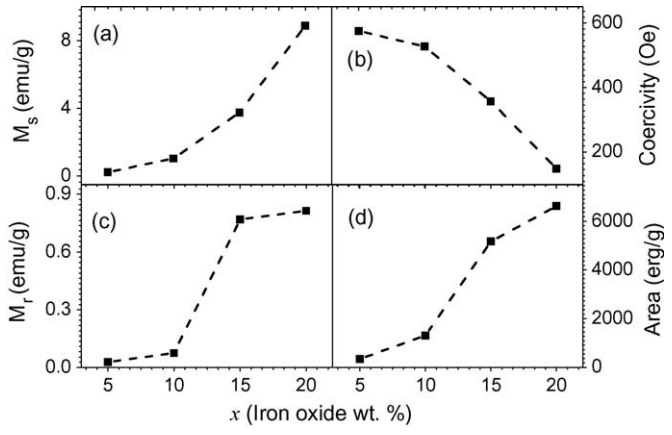

Fig. 3. Variation of room temperature (a) saturation magnetization, (b) coercive field, (c) remanent magnetization, and (d) area under the M–H loop of glass-ceramics as a function of iron oxide content.

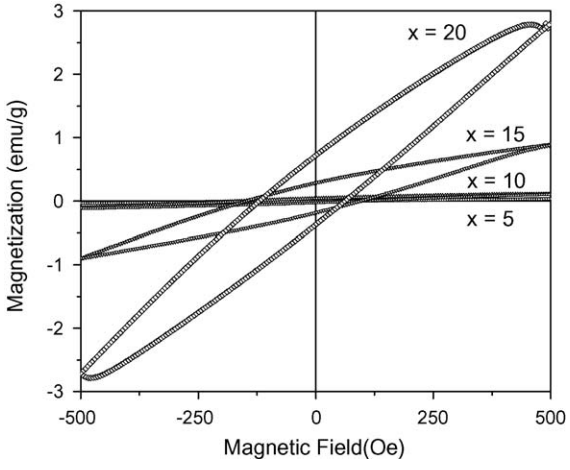

Fig. 4. Room temperature magnetic hysteresis loops of glass-ceramics with different iron oxide concentration under ±500 Oe field sweep.

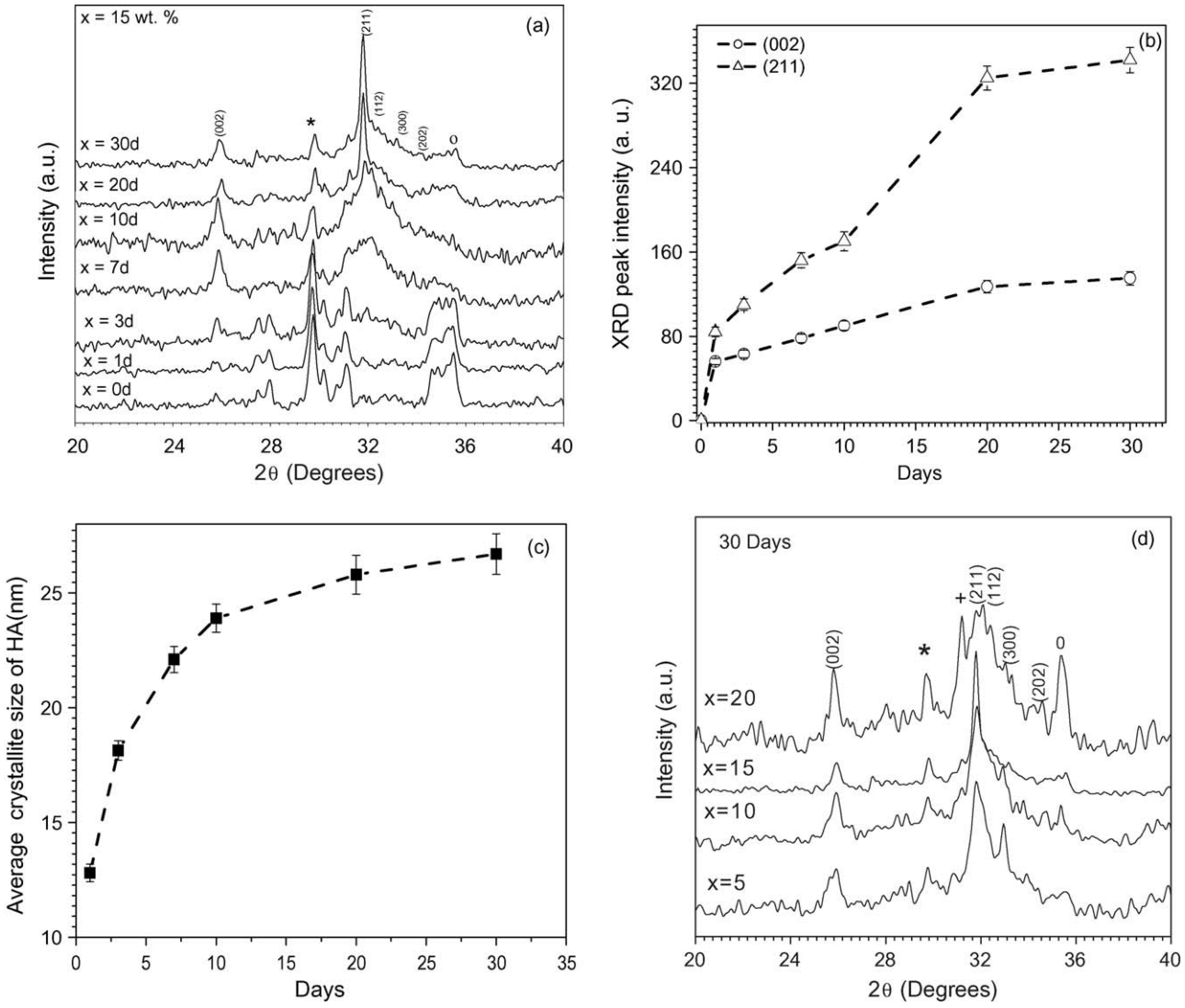

Fig. 5. (a) GI-XRD patterns of the sample with x = 15 wt.% soaked in SBF for different days, (b) GI-XRD intensity of glass sample x = 15 wt.% corresponds to the (0 0 2) and (2 1 1) reflection peak for soaked in SBF for 1, 3, 7, 10, 20 and 30 days, (c) the averages size of HA crystalline (nm) corresponds to the (0 0 2) reflection peak for sample x = 15 wt.% soaked in SBF for 1, 3, 7, 10, 20 and 30 days, and (d) GI-XRD patterns of various compositions of glass-ceramic samples soaked in SBF for 30 days.

oxide before and after soaking in SBF for various time periods (*i.e.* 0, 1, 3, 7, 10, 20 and 30 days). XRD data of the untreated (fresh) sample [designated as 0 d] is shown in Fig. 1. On immersion in SBF for a day or more, new crystalline peaks appear in the GI-XRD patterns, indicating the formation of apatite crystalline layer on the surface of the glass-ceramics. It is obvious from Fig. 5(a) that broad crystalline peaks start to develop in glass-ceramics samples treated with SBF for 3 days or more. Initially, two peaks at 2θ values of $\sim 26^\circ$ and $\sim 32^\circ$ develop after soaking in SBF for a day. The two peaks could be assigned to (0 0 2) and (2 1 1) reflections of HA crystallites (JCPDS file no. 74-0565). The intensities of the (0 0 2) and (2 1 1) reflections of the HA phase increase with an increase in the accumulation of Ca^{2+} and PO_4^{3-} ions on the surface of the glass-ceramics soaked in SBF. The wide diffraction peak spread over 2θ range of 30–34° could be assigned to three closely placed reflections from (1 1 2), (3 0 0) and (2 0 2) planes of the well-crystallized HA phase. The increase in the intensities and decrease in the width of the apatite peaks of the samples immersed for longer periods in SBF clearly shows the evolution of the apatite layer on the surface of the glass-ceramic samples in physiological conditions. Apatite formation on the surface of the glass-ceramics in the SBF is governed by chemical reaction of the surface of the matrix with the fluid. Formation of the apatite layer over the glass-ceramics surface shows that the glass-ceramics samples are bioactive. The gradual growth in the intensity of the individual reflection, appearance of other low intensity apatite reflections and the narrowing of the peak width clearly show the evolution of the crystalline HA surface layer as a function of immersion time in SBF. The intensity of two major reflections, *viz.*, (0 0 2) and (2 1 1), increase [*cf.* Fig. 5(b)] with an increase in the concentration of Ca^{2+} and PO_4^{3-} ions on the surface of the glass immersed in SBF for various days. It is obvious that the intensity of the reflections attain saturated values within 20 days of immersion in SBF. The average size of HA crystallized was calculated from the (0 0 2) reflection using

the Scherrer's formula [29]. Fig. 5(c) reveals an increase in the average particle size of the crystalline surface layer on the glass immersed in SBF for various days, which is consistent with results of reported earlier [24,33]. The crystallite size increases from about 12.8 (±0.38) to 26.7 (±0.69) nm in samples immersed for 3 to 30 days. The size of HA crystalline depends on the rate of crystalline growth on the surface of the glass in the SBF in various days. The variation of the crystallite size with immersion time shows a sharp increase in crystallite size in samples treated in SBF for 10 days, followed by a slower increase in crystallite size in samples treated in SBF for longer time periods.

Fig. 5(d) shows the GI-XRD patterns obtained from the surfaces of glass-ceramics with $x = 5$, 10, 15 and 20 wt.% iron oxide after treatment in SBF for 30 days. The hydroxyapatite (HA) peaks appearing between 2θ values of 30° and 34° sharpen in samples with higher x. Since the broad peaks signify the presence of small sized crystallites, one can infer that on immersion in SBF, the HA formation gradually improves from small sized crystalline aggregates to a well-crystallized HA phase as the amount of iron oxide is increased in the system. Formation of the HA layer over the glass-ceramics surface shows that the glass-ceramics samples are bioactive. The relative intensity and peak width of the characteristic apatite reflections show considerable composition dependence. Addition of Fe_2O_3 in $CaO–SiO_2$ based glass has been reported [26] to reduce its apatite forming ability when immersed in SBF decreased. On the other hand, addition of Na_2O or P_2O_5 facilitates apatite formation in $CaO–SiO_2$ based glasses. Heat-treatment of $CaO–SiO_2$ based glasses containing Fe_2O_3 results in the precipitation of the ferrimagnetic magnetite (Fe_3O_4) crystallites [7,10,12,14]. Such ferrimagnetic bioactive glass-ceramics [7,10,12,14,28,34,35] find potential application as thermoseeds for hyperthermia treatment of cancer. It is interesting to observe the growth in the intensity and reduction in the width of the apatite reflections as a function of increasing iron oxide content in this series of glass-ceramics. As discussed earlier, this might be due to Fe_2O_3 replacing CaO without disturbing the amounts of SiO_2 and P_2O_5 in this series. Such compositional variation seems to aid the apatite forming ability on the surface of these glass-ceramics.

Fig. 6(a) shows the FT-IR spectra of the glass-ceramics sample with $x = 15$ wt.% before and after the immersion in SBF for 0, 1, 3, 7, 10, 20 and 30 days. The spectrum before immersion reveals bands at 1160, 1075, 1025, 890, 815, 636, 570 and 432 cm^{-1}. The peaks at 1160, 1075, 1025, 890, 815, 636, 570 and 432 cm^{-1} correspond [24,36–38] to υ_3 P–O stretching, υ_3 Si–O stretching, υ_3 P–O stretching, Si–O–Si stretching of non-bridging oxygen atoms, Si–O–Si symmetric stretching of bridging oxygen atoms between tetrahedral, O–H stretching, υ_4 P–O bending and υ_4 Si–O–Si bending frequency, respectively. The peak at 1067 cm^{-1}, which is assigned to Si–O stretching vibration in SiO_4 units with bridging oxygen shifts to a lower wave number with longer immersion times and disappears after 3 days of immersion in SBF. As the peak at 1067 cm^{-1} shifts and disappears a new vibrational mode is observed at 1030 cm^{-1}, which can be assigned to Si–O bond vibration between two SiO_4

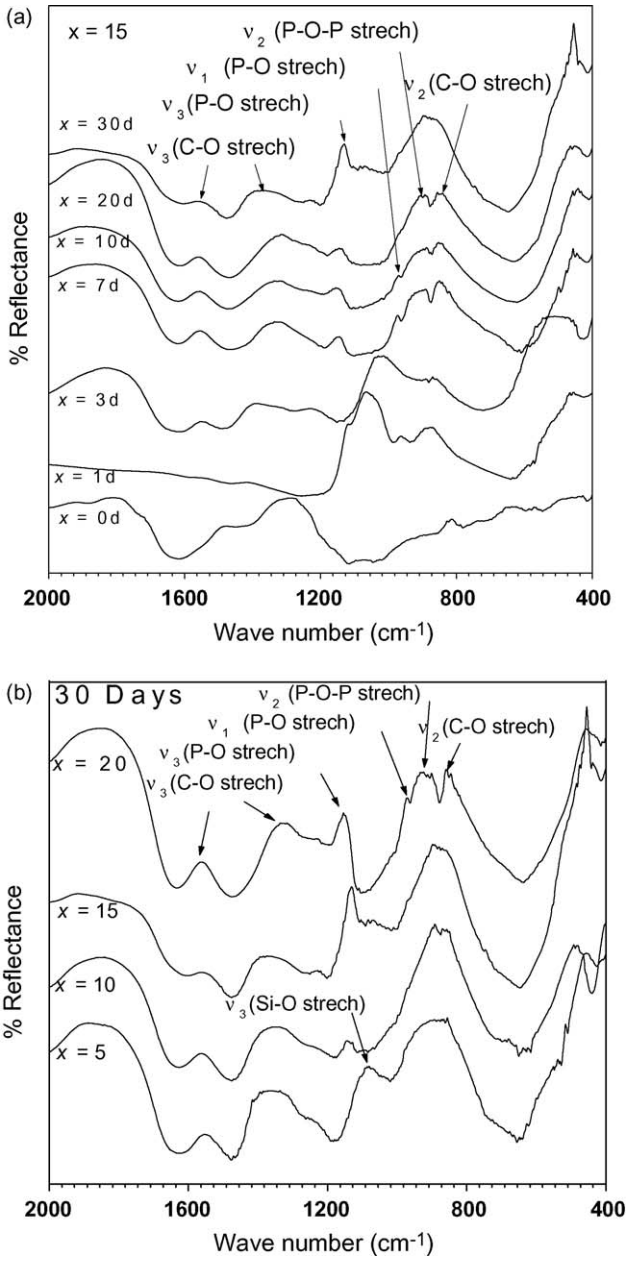

Fig. 6. (a) FT-IR spectra of samples with $x = 15$ wt.% soaked in SBF for different days, and (b) FT-IR spectra of the surfaces of various glass-ceramics soaked in SBF for 30 days.

tetrahedra. After 1 day of immersion, new bands start developing at 457, 860, 902, 970, 1145, 1227, 1327 and 1556 cm^{-1}. The peaks at 457 and 902 cm^{-1} correspond to υ_2 P–O bending and υ_1 P–O–P stretching frequency, respectively. The band located at 860 cm^{-1} and the broad bands at 1327 and 1556 cm^{-1} can be assigned to C–O vibration mode in CO_3^{2-}. These bands signify the incorporation of carbonate anions from the SBF in the apatite crystal lattice. After immersion for a day, the appearance of bands at 970 and 1140 cm^{-1} can be seen, which are related to the calcium phosphate (hydroxyl apatite) surface layer. The peak at 1140 cm^{-1} is associated with the υ_3 P–O stretching mode. With further increase in immersion time, the intensity of the bands due to υ_3 P–O stretching mode increases. The peak at 970 cm^{-1} reflects the υ_1 P–O symmetric stretching mode. This band

indicates the obviation of phosphate ions from the ideal tetrahedral structure. This is a Raman active only mode when v_1 P–O symmetric stretch is in the free ion state. This Raman active mode can be seen in the infrared spectra because of the lowering of the symmetry in the crystalline state. With further increase in immersion time, the intensity of the bands due to CO_3^{2-} increases. Carbonate ions occupy two different sites in carbonated apatite: peaks in the region of 1650–1300 cm^{-1} are due to v_3 vibrational mode, whereas the peak at 860 cm^{-1} is due to the v_2 vibrational mode [38] of carbonate ion. The v_3 band splits into two peaks centered at 1327 and 1556 cm^{-1}, respectively, with the distribution of the carbonate v_3 sites depending on the maturation and formation of apatite crystals. Occupancy of the v_2 sites is considered to occur competitively between the OH^{-1} and carbonate groups at the interface of growing crystal, whereas occupancy of the v_3 sites depends on competition between the phosphates and carbonate ions [38]. Presence of v_2 and v_3 vibrational modes of carbonate is the imprint of the development of an HCA layer on the surface of the sample.

Fig. 6(b) shows the FT-IR reflection spectra of each glass-ceramic composition after the immersion in SBF for 30 days. Spectral bands of HA assigned to PO_4^{3-} groups (v_3 – 1145 cm^{-1}, v_1 – 970 cm^{-1}, v_1 – 902 cm^{-1} and v_2 – 457 cm^{-1}) and CO_3^{2-} functional groups (v_2 – 860 cm^{-1}, v_3 – 1327 $cm^{-1}$and v_3 – 1556 cm^{-1}) appear in the spectra. The band at 1040 cm^{-1} v_3 Si–O stretch disappears in the samples with x = 15 and 20 wt.%. The peak at 905 cm^{-1} reflects the v_1 P–O–P stretching mode. These bands (1145, 902, 860) sharpen and their relative intensities increase with an increase in iron oxide content signifying the formation of a well-crystallized HCA layer in these samples. The FT-IR studies thus clearly show an increased bioactivity in these glass-ceramics as the iron oxide content is increased in the composition range studied.

Fig. 7(a) shows the SEM micrographs of the glass-ceramic sample with x = 15 wt.% after immersion in SBF for 1, 3, 7, 10,

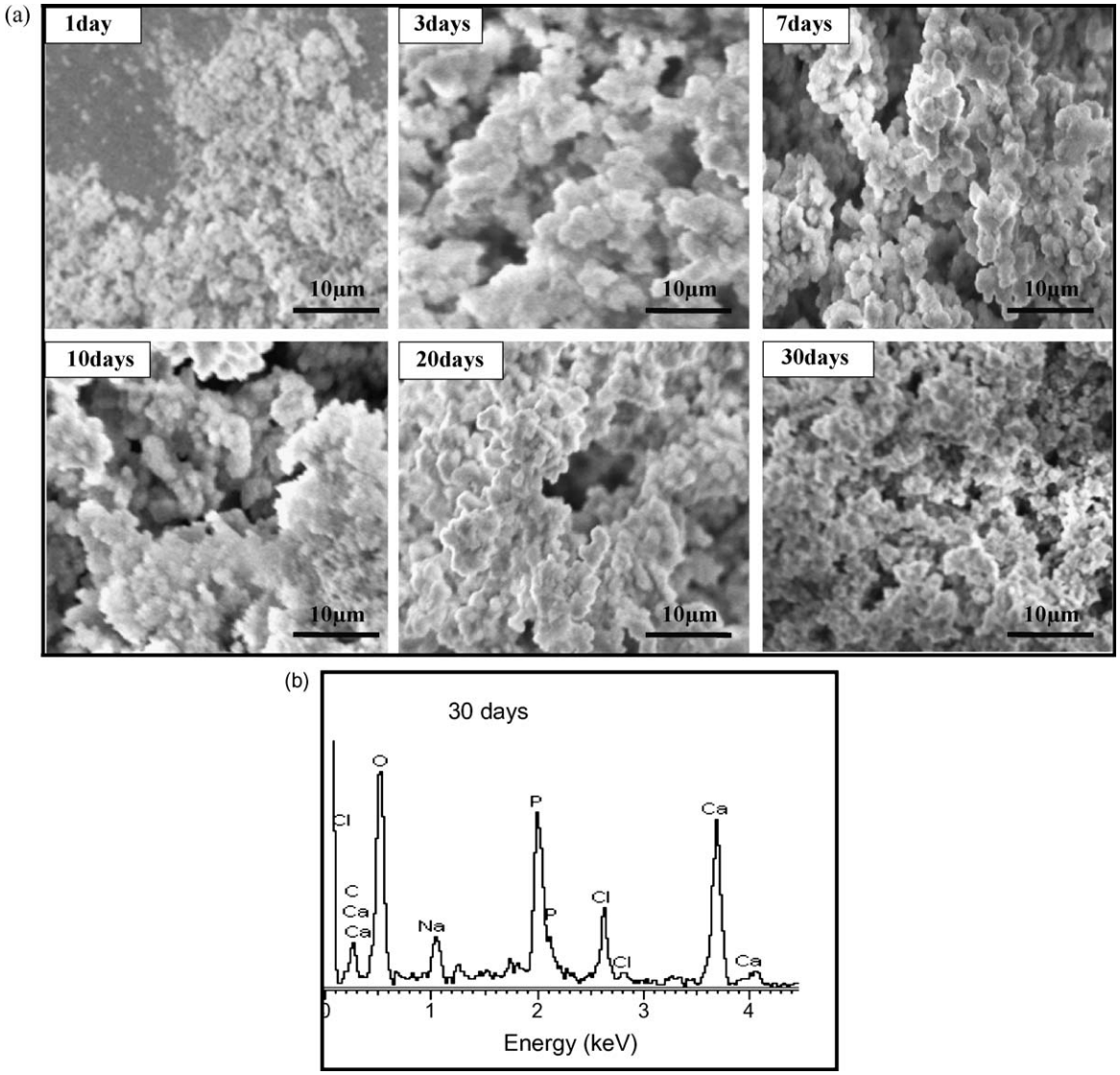

Fig. 7. (a) SEM micrographs of the surfaces of glass-ceramic sample with x = 15 wt.% soaked in SBF for various days (magnification: 1000×) and (b) EDS spectra of x = 15 wt.% soaked in SBF for 30 days.

20 and 30 days, respectively. The micrographs have been obtained under 1000× magnification. The micrographs provide visual evidence of the formation of a surface layer on the bioglass-ceramics, which can now be presumed to be an apatite layer. After 30 days of immersion, the whole surface of the specimen is covered with spherical Ca–P particulate apatite layer. Energy dispersive spectrometer (EDS) composition analysis reveals the gradual development of hydroxycarbonate apatite on the surface of glass-ceramics samples after immersion for various time periods in SBF. The spherical particles observed in the sample treated in SBF for 30 days are made up of calcium and phosphorus with Ca/P molar ratio (calculated from EDS analysis) of ∼1.67, which is close to the value in HA. Microanalysis of the precipitates reveals the presence of small quantities of Na and Cl as shown in the EDS spectra in Fig. 7(b). This finding is in agreement with reports which claim that the growth of HA in SBF is accompanied by the incorporation of sodium, magnesium and chlorine ions [39] as well. It may thus be concluded that the surface layer contains carbonate, sodium, magnesium and chlorine substituted hydroxyapatite [24,40].

4. Conclusion

In vitro bioactivity studies on $4.5MgO(45-x)$-$CaO34SiO_2 16P_2O_5 0.5CaF_2 x Fe_2O_3$ $(5 \leq x \leq 20)$ glass-ceramics containing 5–20 wt.% of Fe_2O_3 shows that these materials are capable of bonding with the human bone. FT-IR measurements demonstrate the presence of CO_3^{2-} group and hence hydroxycarbonate apatite appearance on SBF treated sample surface. EDS analysis shows that the Ca/P ratio ∼1.67 in samples dowsed for 30 days in SBF. Hydroxyapatite and wollastonite are the major biocompatible crystalline phases found in the MBCs. Nanocrystalline magnetite crystallized as a third phase with its size strongly dependent on the iron oxide content of the MBCs. Magnetic properties and heat generation capability of the MBCs under high and clinically amenable magnetic fields have been evaluated. The results reported in this paper show that bioactivity increases when the iron content is increased. Thus, compositions with higher iron oxide content contain higher amounts of bone mineral phases as well as the magnetic phase. The higher VHN of these magnetic bioactive glass-ceramics gives them an advantage over CaO based magnetic bioactive glass-ceramics due to their higher load bearing capacity.

Acknowledgements

Financial assistance from the Department of Science and Technology, India *vide* project No: SR/S2/CMP-19/2006 are gratefully acknowledged.

References

[1] M. Jarcho, J.L. Kay, R.H. Gumaer, H.P. Drobeck, Tissue, cellular and subcellular events at bone-ceramic hydroxyapatite interface, J. Bioeng. 1 (1977) 79–92.
[2] R.Z. LeGeros, J.P. LeGeros, in: L.L. Hench, J. Wilson (Eds.), An Introduction to Bioceramics, World Scientific Publishing Co. Pte. Ltd., Singapore, 1993, p. 139.
[3] T. Kokubo, S. Ito, S. Sakka, T. Yamamuro, Formation of a high-strength bioactive glass-ceramic in the system $MgO–CaO–SiO_2–P_2O_5$, J. Mater. Sci. 21 (1986) 536–540.
[4] T. Kitsugi, T. Yamamuro, T. Nakamura, T. Kokubo, Bone bonding behavior of $MgO–CaO–SiO_2–P_2O_5–CaF_2$ glass (mother glass of A–W-glass-ceramics), J. Biomed. Mater. Res. 23 (1989) 631–648.
[5] T. Nakamuro, T. Yamamuro, S. Higashi, T. Kokubo, S. Ito, A new glass-ceramic for bone replacement: evaluation of its bonding to bone tissue, J. Biomed. Mater. Res. 19 (1985) 685–698.
[6] M. Ikenaga, K. Ohura, T. Nakamura, Y. Kotoura, T. Yamamuro, M. Oka, Y. Ebisawa, T. Kokubo, Hyperthermic treatment of experimental bone tumours with a bioactive ferromagnetic glass-ceramic, Bioceramics 4 (1991) 255–262.
[7] K. Ohura, M. Ikenaga, T. Nakamura, T. Yamamuro, Y. Ebisawa, T. Kokubo, Y. Kotoura, M. Oka, A heat-generating bioactive glass-ceramic for hyperthermia, J. Appl. Biomater. 2 (1991) 153–159.
[8] T. Kokubo, Y. Ebisawa, Y. Sugimoto, M. Kiyama, K. Ohura, T. Yamamuro, M. Hiraoka, M. Abe, Preparation of bioactive and ferromagnetic glass-ceramic for hyperthermia, Bioceramics 5 (1992) 213–223.
[9] M. Kawashita, Y. Iwahashi, T. Kokubo, T. Yao, S. Hamada, T. Shinjo, Preparation of glass-ceramics containing ferrimagnetic zinc–iron ferrite for the hyperthermal treatment of cancer, J. Ceram. Soc. Jpn. 112 (2004) 373–379.
[10] T. Leventouri, A.C. Kis, J.R. Thompson, I.M. Anderson, Structure, microstructure, and magnetism in ferromagnetic bioceramics, Biomaterials 26 (2005) 4924–4931.
[11] O. Bretcanu, S. Spriano, E. Verne, M. Coisson, P. Tiberto, P. Allia, The influence of crystallized Fe_3O_4 on the magnetic properties of coprecipitation-derived ferrimagnetic glass-ceramics, Acta Biomater. 1 (2005) 421–429.
[12] R.K. Singh, G.P. Kothiyal, A. Srinivasan, Magnetic and structural properties of $CaO–SiO_2.P_2O_5–Na_2O–Fe_2O_3$ glass ceramics, J. Magn. Magn. Mater. 320 (2008) 1352–1356.
[13] M. Kawashita, H. Takaoka, T. Kokubo, T. Yao, S. Hamada, T. Shinjo, Preparation of magnetite-containing glass-ceramics in controlled atmosphere for hyperthermia of cancer, J. Ceram. Soc. Jpn. 109 (2001) 39–44.
[14] Y. Ebisawa, F. Miyaji, T. Kokubo, K. Ohura, T. Nakamura, Bioactivity of ferromagnetic glass-ceramics in the system $FeO–Fe_2O_3–CaO–SiO_2$, Biomaterials 18 (1997) 1277–1284.
[15] K. Ohura, T. Nakamura, T. Yamamuro, T. Kokubo, Y. Ebisawa, Y. Kotoura, M. Oka, Bone bonding ability of P_2O_5-free $CaO·SiO_2$ glasses, J. Biomed. Mater. Res. 25 (1991) 357–365.
[16] K.H. Karlsson, K. Froberg, T. Ringbom, A structural approach to bone adhering of bioactive glasses, J. Non-Cryst. Solids 112 (1989) 69–72.
[17] T. Kitsugi, T. Yamamuro, T. Nakamura, S. Higashi, Y. Kakutani, K. Hyakuna, S. Ito, T. Kokubo, M. Takagi, T. Shibuya, Bone bonding behavior of three kinds of apatite-containing glass-ceramics, J. Biomed. Mater. Res. 20 (1986) 1295–1307.
[18] T. Kitsugi, T. Nakamura, T. Yamamuro, T. Kokubo, T. Shibuya, M. Takagi, SEM-EPMA observation of three types of apatite-containing glass-ceramics implanted in bone: the variance of Ca–P rich layer, J. Biomed. Mater. Res. 21 (1987) 1255–1271.
[19] C. Ohtsuki, H. Kushitani, T. Kokubo, S. Kotani, T. Yamamuro, Apatite formation on the surface of Ceravital-type glass-ceramic in the body, J. Biomed. Mater. Res. 95 (1991) 1363–1370.
[20] H.M. Kim, F. Miyaji, T. Kokubo, Bioactivity of $Na_2O–CaO–SiO_2$ glasses, J. Am. Ceram. Soc. 78 (1995) 2405–2411.
[21] C. Ohtsuki, T. Kokubo, T. Yamamuro, Mechanism of apatite formation on $CaO–SiO_2–P_2O_5$ glasses in a simulated body fluid, J. Non-Cryst. Solids 143 (1992) 84–92.
[22] M.R. Filgueiras, G.R. Torre, L.L. Hench, Solution effects on the surface reaction of a bioactive glass, J. Biomed. Mater. Res. 27 (1993) 445–453.
[23] T. Kokubo, H. Kushitani, S. Sakka, T. Kitsugi, T. Yamamuro, Solutions able to reproduce in vivo surface-structure changes in bioactive glass ceramic A–W, J. Biomed. Mater. Res. 24 (1990) 721–734.

[24] R.K. Singh, G.P. Kothiyal, A. Srinivasan, In vitro evaluation of bioactivity of $CaO–SiO_2–P_2O_5–Na_2O–Fe_2O_3$ glasses, Appl. Surf. Sci. 255 (2009) 6827–6831.
[25] Y. Ebisawa, T. Kokubo, K. Ohura, T. Yamamuro, Bioactivity of $CaO·SiO_2$-based glasses: in vitro evaluation, J. Mater. Sci. Mater. Med. 1 (1990) 239–244.
[26] T. Kokubo, S. Ito, Z.T. Huang, T. Hayashi, S. Sakka, T. Kitsugi, T. Yamamuro, Ca, P-rich layer formed on high-strength bioactive glass-ceramic A–W, J. Biomed. Mater. Res. 24 (1990) 331–343.
[27] R.K. Singh, G.P. Kothiyal, A. Srinivasan, Bioactivity of $CaO–SiO_2–P_2O_5–Na_2O–Fe_2O_3$ glass-ceramics: in vitro evaluation, Arch. Bioceram. Res. 8 (2008) 89–92.
[28] K. Ohura, T. Nakamura, T. Yamamuro, Y. Ebisawa, T. Kokubo, Y. Kotoura, M. Oka, Bioactivity of $CaO·SiO_2$ glasses added with various ions, J. Mater. Sci. Mater. Med. 3 (1992) 95–100.
[29] B.D. Cullity, Elements of X-ray Diffraction, Addison-Wesley, Reading, 1978.
[30] R.K. Singh, A. Dixit, S. Sarma, P.S. Robi, K. Sharma, G.P. Kothiyal, A. Srinivasan, Synthesis & preliminary characterization of a new class of glass-ceramics for hyperthermia treatment application, in: Proc. Natl. Symp. Sci. & Tech. Glass/Glass-Ceram, Mumbai, 2006, 123–124.
[31] R.K. Singh, G.P. Kothiyal, A. Srinivasan, Studies on new bioglasses and bioglass-ceramics containing Fe_3O_4, in: Proc. DAE-SSP Symp. India, vol. 51, 2006, 411–412.
[32] R.D. Cullity, Introduction to Magnetic Materials, Addison-Wesley, Reading, 1972.
[33] C. Li-Yun, Z. Chuan-Bo, H. Jian-Feng, Influence of temperature, $[Ca^{2+}]$, Ca/P ratio and ultrasonic power on the crystallinity and morphology of hydroxyapatite nanoparticles prepared with a novel ultrasonic precipitation method, Mater. Lett. 59 (2005) 1902–1906.
[34] O. Bretcanu, S. Spriano, C.B. Vitale, E. Verne, Synthesis and characterization of coprecipitation-derived ferrimagnetic glass-ceramic, J. Mater. Sci. 41 (2006) 1029–1037.
[35] O. Bretcanu, E. Verne, M. Coisson, P. Tiberto, P. Allia, Magnetic properties of the ferrimagnetic glass ceramics for hyperthermia, J. Magn. Magn. Mater. 305 (2006) 529–533.
[36] C.Y. Kim, A.E. Clark, L.L. Hench, Early Stages of calcium phosphate layer formation in bioglasses, J. Non-Cryst. Solids 113 (1989) 195–202.
[37] C.C. Silva, M.A. Valente, M.P.F. Graca, A.S.B. Sombra, Preparation and optical characterization of hydroxyapatite and ceramic systems with titanium and zirconium formed by dry high-energy mechanical alloying, Solid State Sci. 6 (2004) 1365–1374.
[38] I. Rehman, W. Bonfield, Characterization of hydroxyapatite and carbonated apatite by photo acoustic FTIR spectroscopy, J. Mater. Sci. Mater. Med. 8 (1997) 1–4.
[39] S.V. Dorozhkin, E.I. Dorozhkina, M. Epple, Precipitation of carbonateapatite from a revised simulated body fluid in the presence of glucose, J. Appl. Biomater. Biomech. 1 (2003) 200–2007.
[40] J. Barralet, S. Best, W. Bonfield, Carbonate substitution in precipitated hydroxyapatite: an investigation into the effects of reaction temperature and bicarbonate ion concentration, J. Biomed. Mater. Res. 41 (1998) 79–86.